Toughness of Ni/Al$_2$O$_3$ interfaces as dependent on micron-scale plasticity and atomistic-scale separation

Y. Wei[a] and J.W. Hutchinson[b]*

[a]LNM, Institute of Mechanics, Chinese Academy of Sciences, Beijing, China; [b]School of Engineering and Applied Sciences, Harvard University, Cambridge, MA, USA

Ceramic/metal interfaces were studied that fail by atomistic separation accompanied by plastic dissipation in the metal. The macroscopic toughness of the specific Ni alloy/Al$_2$O$_3$ interface considered is typically on the order of ten times the atomistic work of separation in mode I and even higher if combinations of mode I and mode II act on the interface. Inputs to the computational model of interface toughness are: (i) strain gradient plasticity applied to the Ni alloy with a length parameter determined by an indentation test, and (ii) a potential characterizing mixed mode separation of the interface fit to atomistic results. The roles of the several length parameters in the strain gradient plasticity are determined for indentation and crack growth. One of the parameters is shown to be of dominant importance, thus establishing that indentation can be used to measure the relevant length parameter. Recent results for separation of Ni/Al$_2$O$_3$ interfaces computed by atomistic methods are reviewed, including a set of results computed for mixed mode separation. An approximate potential fit to these results is characterized by the work of separation, the peak separation stress for normal separation and the traction–displacement relation in pure shearing of the interface. With these inputs, the model for steady-state crack growth is used to compute the toughness of the interface under mode I and under the full range of mode mix. The effect of interface strength and the work of separation on macroscopic toughness is computed. Fundamental implications for plasticity-enhanced toughness emerge.

Keywords: fracture; plasticity; work of separation; atomistic separation; ceramic–metal interface

1. Introduction

Thermal barrier coatings used to protect metallic components exposed to the highest temperatures in aircraft and power generation turbines are multilayers of a porous ceramic layer with low thermal conductivity overlying a very thin, fully dense layer of Al$_2$O$_3$ that forms from, and adheres to, a metal layer, termed the bond coat, that bonds to the component. The coatings are dual purpose in that the Al$_2$O$_3$ layer serves as an oxidation barrier. Typically, the coatings experience temperature changes of over 1000 K in each operation cycle. Thermal expansion mismatch between the ceramic layers and the thicker metallic component produces large compressive stresses in the ceramic layers upon

---

*Corresponding author. Email: hutchinson@husm.harvard.edu

cool-down. After sufficiently severe thermal cycling, the coatings develop a susceptibility to delamination and spalling driven by these stresses.

Many thermal barrier systems employ a class of Ni alloy bond coats commonly denoted by NiCoCrAlY. Delamination of these systems usually occurs by fracture upon cool-down along the interface between the Ni alloy bond coat and the Al_2O_3 layer [1]. The focus of this paper is the room temperature toughness of this interface and, in particular, on how this toughness relates to interface separation at the atomistic scale. The interface is believed to deteriorate as the component is thermally cycled due to migration of segregates to the interface and possible changes in bond coat composition. The present study will make contact with recent atomistic modelling of Ni/Al_2O_3 interfaces [2,3].

Plasticity induced by the crack in the Ni alloy makes a major contribution to the toughness of Ni alloy/Al_2O_3 interfaces, typically enhancing the atomistic work of separation by a factor on the order of ten. This multiplicative enhancement is studied in this paper with emphasis on the interaction between interface separation and plasticity. A model is proposed that links the macroscopic scale relevant to the interface toughness through the zone of plasticity to the interface where separation occurs at the atomic scale. The model [4] is a descendant of a series of earlier models that attempt to capture the nonlinear coupling between the work of separation and plastic dissipation [5–8].

Ni alloy/Al_2O_3 interfaces are relatively brittle and not strong enough to emit dislocations in the separation process. Thus, the plasticity accompanying interface cracking is due to generation and movement of dislocations within the metal. At room temperature the bulk Ni-alloy has a high yield stress ($\sim$700 MPa) and, as will be seen, the size of the plastic zone is less than one micron. Nevertheless, plastic dissipation accompanying interface separation can account for 90% or more of the total fracture energy. Another consequence of the small size of the plastic zone is that conventional, or "bulk", plasticity theory cannot be used in the model. Instead, strain gradient plasticity will be used to describe the strong size dependence associated with plasticity at the micron and sub-micron scale. This plasticity theory brings in material length parameters not present in conventional theory. Issues related to these parameters are addressed related to their use in crack growth. It is also established that indentation can be used to measure the most important length parameter.

Most emphasis in this paper is on mode I interface toughness, but mixed mode toughness trends will also be determined because of their relevance to delamination of the thermal barrier coatings. The toughness model requires that separation at the atomic scale be characterized under mixed mode conditions, and we will make use of some preliminary atomistic results for mixed mode separation histories obtained for the first time.

The model used to compute the interface toughness is depicted in Figure 1 with the metal (the Ni alloy) above the interface and the ceramic (Al_2O_3) below. Plane strain deformation is assumed. The elastic properties of the metal and the ceramic are taken to be linear and isotropic with Young's modulus and Poisson's ratio, (E_1, ν_1) and (E_2, ν_2), respectively, as noted in Figure 1. The metal is characterized by strain gradient plasticity which is specified in the next section. In addition to the initial tensile yield stress, σ_Y, and the strain hardening exponent, N, as defined conventionally in terms of tensile data, strain gradient plasticity requires specification of a length parameter, ℓ, typically on the order of a micron or less, that determines the size-dependent hardening associated with plastic strain gradients.
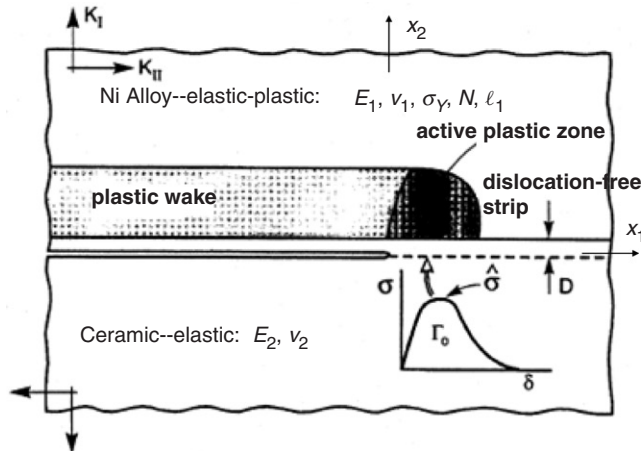
Figure 1. Unified model for steady-state crack growth in small scale yielding. Crack growth occurs along the interface between the Ni alloy and the Al$_2$O$_3$. A traction–separation relation links the two materials across the interface. The ceramic is taken to be elastic, whereas the metal is characterized by strain-gradient plasticity with the parameters listed above. The model includes a dislocation-free strip of height D above the interface, which will be eliminated in most of the computations.

The metal and the ceramic blocks above and below the interface along the x_1 coordinate axis are linked by a traction–separation relation that requires specification of the dependence of the two traction components, $(T_1, T_2) = (\sigma_{12}, \sigma_{22})$, on the two components, (δ_1, δ_2), of the displacement of the top face relative to the bottom face of the interface. Atomistic calculations for normal, shear and mixed mode separation of the Ni/Al$_2$O$_3$ interface [3] will be presented in Section 3, and the potential used to generate the traction–separation relation introduced below will be fit to the atomistic results. The potential is essentially the same as that proposed by Sun et al. [9] and similar to an earlier more restricted version [10]. In the present notation, the potential is defined as

$$W(\delta_1, \delta_2) = \Gamma_0 \left[1 - \left(1 + \frac{\delta_2}{\hat{\delta}} \right) \exp\left(-\frac{\delta_2}{\hat{\delta}} \right) + f(\delta_1) \left[1 + (1+\beta)\frac{\delta_2}{\hat{\delta}} \right] \exp\left(-\frac{\delta_2}{\hat{\delta}} \right) \right]. \quad (1)$$

Tractions are given by

$$
\begin{aligned}
T_1 &= \frac{\partial W}{\partial \delta_1} = \Gamma_0 \frac{\mathrm{d}f(\delta_1)}{\mathrm{d}\delta_1} \left[1 + (1+\beta)\frac{\delta_2}{\hat{\delta}} \right] \exp\left(-\frac{\delta_2}{\hat{\delta}} \right), \\
T_2 &= \frac{\partial W}{\partial \delta_2} = \frac{\Gamma_0}{\hat{\delta}} \left[\frac{\delta_2}{\hat{\delta}} - \left((1+\beta)\frac{\delta_2}{\hat{\delta}} - \beta \right) f(\delta_1) \right] \exp\left(-\frac{\delta_2}{\hat{\delta}} \right).
\end{aligned}
\quad (2)
$$

The work of separation/area, Γ_0, is path-independent. For purely normal separation ($\delta_1 = 0, \delta_2 > 0$), Equation (2) reduces to the "universal" separation function [11], $T_2 = (\Gamma_0/\hat{\delta})(\delta_2/\hat{\delta}) \exp(-\delta_2/\hat{\delta})$, which has been shown to accurately represent atomistic computations for many interfaces. For normal separation, the maximum traction, $\hat{\sigma} = (T_2)_{\max}$, is attained at $\delta_2 = \hat{\delta}$ and is given by

$$\hat{\sigma} = \frac{\Gamma_0}{e\hat{\delta}}. \quad (3)$$

For constrained shear of the interface ($\delta_1 > 0$, $\delta_2 = 0$), Equation (2) gives

$$T_1 = \Gamma_0 \frac{\mathrm{d}f(\delta_1)}{\mathrm{d}\delta_1}, \quad T_2 = \beta \frac{\Gamma_0}{\hat{\delta}} f(\delta_1). \tag{4}$$

For unconstrained shear ($\delta_1 > 0$, $T_2 = 0$), T_1 is given by the first of Equation (2) with

$$\frac{\delta_2}{\hat{\delta}} = -\frac{\beta f(\delta_1)}{1 - (1 + \beta)f(\delta_1)}. \tag{5}$$

Three parameters, Γ_0, $\hat{\delta}$ and β, and one function, $f(\delta_1)$, specify the potential. In this paper, Γ_0 and $\hat{\delta}$, or, equivalently, $\hat{\sigma}$, will be fit to normal separation data. Data for constrained pure shear, denoted by $T_1^{II}(\delta_1)$, will be used in conjunction with the first of Equations (4) to determine $f(\delta_1)$. The parameter β determines the coupling between the normal stress in pure shear. With $\beta = 0$, coupling vanishes such that the cases of unconstrained and constrained shear become identical. Note that in constrained shear the interface potential reduces to $W = \Gamma_0 f(\delta_1)$, and it follows that $f(\delta_1)$ is inherently non-negative with $f(0) = 0$. Thus, from the second of Equations (4) it is seen that constrained shear produces tension across the interface if $\beta > 0$ and compression if $\beta < 0$. The influence of this parameter will be explored. The difference between the present potential and the earlier version [9] is only that the former was restricted to shear tractions in the shape of a sine function; the version in [10] was further restricted to $\beta = 0$.

Illustrative examples in which the potential, Equation (1), is fit to atomistic results for the Ni/Al$_2$O$_3$ interface will be given in Section 3, where it will also be shown that the potential appears to capture mixed mode separation with reasonable fidelity.

The interface toughness model in Figure 1 assumes small scale yielding with plasticity confined to the crack tip and to the wake of plastically deformed metal in the unloaded region behind the advancing crack tip. Steady-state conditions are invoked under the assumption that the crack has already propagated a distance many times the plastic zone size such that the fields are not changing for an observer advancing with the tip. The model shown in Figure 1 includes a dislocation-free zone around the crack tip, taken as a thin strip of thickness D separating the crack tip from any plastic deformation as introduced in earlier models [5,7]. These models employed a critical energy release rate associated with the crack-tip singularity within the elastic strip as the propagation criterion. The "unified model" [4] in Figure 1 also incorporates the dislocation-free strip. However, crack advance is controlled by the cohesive law, Equations (1)–(2). Strain gradient plasticity plays an essential role in the model by elevating the tractions acting on the interface, and a very thin dislocation-free strip has almost no influence on the interface toughness of Ni alloy/Al$_2$O$_3$ systems and can be deleted from the model.

The remote elastic field imposed at a radial distance R_{remote} from the crack tip is specified by the mode I and II stress intensity factors (K_I, K_{II}). The remote energy release rate characterizing the total energy being dissipated at the crack tip is given by

$$G = \frac{1}{2}\left(1 - \beta_D^2\right)\left(\frac{1 - \nu_1^2}{E_1} + \frac{1 - \nu_2^2}{E_2}\right)\left(K_I^2 + K_{II}^2\right), \tag{6}$$

where β_D is the second Dundurs' elastic mismatch parameter defined later. As described in previous papers [4,12], the steady-state formulation requires integration over paths travelled by material particles to determine the deformation history within the active

plastic zone and in the wake due to the path dependence of plasticity. Iteration is required to meet the growth conditions consistent with steady-state. In the iteration process, the remote intensity factors are adjusted until the critical separation conditions along the interface ahead of the tip are met. When critical conditions are met, the toughness of the interface is defined as $\Gamma_{SS} = G$ with G given by Equation (6). Details of these procedures and of the finite element method used in the numerical model are described in the aforementioned papers and by Wei [13]. The size of smallest elements in the mesh in vicinity of the crack tip is approximately $\hat{\delta}/2$.

The dependence of the interface toughness on the relative amount of mode II to mode I, $\Gamma_{SS}(\psi)$, will also be explored in this paper and, for this purpose, the standard measure of the mode mix will be used:

$$\psi = \tan^{-1}\left(\frac{K_{\mathrm{II}}}{K_{\mathrm{I}}}\right). \tag{7}$$

An important length parameter in the model [6] is

$$R_0 = \frac{1}{3\pi(1 - v^2)} \frac{E_1\Gamma_0}{\sigma_Y^2} . \tag{8}$$

Under mode I conditions, the reference length R_0 is an estimate of the height of the active plastic zone when the amplitude of the remote field is set at $G = \Gamma_0$. The height of the actual plastic zone is a computed quantity that scales with $(\Gamma_{SS}/\Gamma_0)R_0$ and also depends on ψ.

We summarize this section by collecting all the parameters introduced above in dimensionless form in an expression for steady-state toughness as predicted by the model,

$$\frac{\Gamma_{SS}}{\Gamma_0} = F\left(\psi, \frac{\hat{\sigma}}{\sigma_Y}, \frac{\ell}{R_0}, N, \frac{D}{R_0}, \frac{E_1}{E_2}, \frac{\sigma_Y}{E_1}, v_1, v_2\right), \tag{9}$$

of the nine dimensionless variables, the first four in Equation (9) are of primary importance. Not shown, but implicitly involved, are the parameter β and the function $f(\delta_1)$ describing pure shear of the interface. A dimensionless ratio such as $\hat{\delta}/\ell$ can be re-expressed in terms of the variables in Equation (9) using Equation (3).

2. Strain gradient plasticity applied to indentation and crack growth

Strong scale effects arise when plastic deformation takes place in the micron and sub-micron range. For indentation, this is manifest by the fact that the measured hardness of a metal is larger the smaller the indent size. According to conventional "bulk" plasticity hardness should be independent of indent size. In crack growth, the scale effect produces stresses within distances of microns or less from the crack tip that are significantly elevated above those expected on the basis of conventional plasticity. Both effects are attributed to hardening due to geometrically necessary dislocations accompanying strain gradients at the micron to sub-micron scale [14]. Stress elevation plays an essential role in separating the metal/ceramic interface of interest in this paper. The phenomenological theory of strain gradient plasticity introduced by Fleck and Hutchinson [15] will be used to represent the behaviour of the Ni alloy. The constitutive model invokes isotropic hardening and introduces three length parameters, ℓ_1, ℓ_2 and ℓ_3, detailed below, which characterize the

material's behavior. Thus, in addition to measurements required to measure the metal's uniaxial stress–strain curve as input to the plasticity theory, additional measurements are required to determine the length parameters. In this section it will be established that one of the three length parameters is of dominant importance in indentation and crack growth. Consequently, indentation is likely to be the most effective means of measuring this parameter.

2.1. *The strain gradient plasticity constitutive model*

Throughout this paper the uniaxial stress–strain behavior of the metal is taken to be a piecewise power law specified in uniaxial tension by

$$
\begin{aligned}
\sigma &= E_1 \varepsilon, && \varepsilon \leq \varepsilon_Y \\
\sigma &= \sigma_Y \left(\frac{\varepsilon}{\varepsilon_Y} \right)^N, && \varepsilon > \varepsilon_Y,
\end{aligned}
\tag{10}
$$

where E_1 is Young's modulus and $\sigma_Y = E_1 \varepsilon_Y$ connects the initial yield stress and strain. As already indicated, the elastic behavior for both the metal and the ceramic is taken to be linear and isotropic. The effective plastic strain-rate of the metal is defined as standard by

$$
\dot{\varepsilon}_P = \sqrt{\frac{2}{3} \dot{\varepsilon}_{ij}^P \dot{\varepsilon}_{ij}^P},
\tag{11}
$$

where the plastic strain-rate, $\dot{\varepsilon}_{ij}^P$, is incompressible, i.e. $\dot{\varepsilon}_{jj}^P = 0$. The constitutive model is an isotropic, phenomenological relation based on a generalized effective plastic strain-rate defined in terms of $\dot{\varepsilon}_P$ and the three quadratic invariants of the gradient of the plastic strain-rate, $\rho_{ijk} = \rho_{jik} = \dot{\varepsilon}_{ij,k}^P$. With $\rho_{ijk}^S = (1/3)(\rho_{ijk} + \rho_{jki} + \rho_{kij})$, $\chi_{ij} = e_{iqr}\rho_{jrq}$ and e_{ijk} as the permutation tensor, the three invariants of the strain-rate gradients are $I_1 = \rho_{ijk}^S \rho_{ijk}^S - (4/15)\rho_{kii}\rho_{kjj}$, $I_2 = (1/3)(\chi_{ij}\chi_{ij} + \chi_{ij}\chi_{ji})$, $I_3 = (3/5)(\chi_{ij}\chi_{ij} - \chi_{ij}\chi_{ji})$. The generalized effective plastic strain-rate is defined as

$$
\dot{E}_P^2 = \dot{\varepsilon}_P^2 + \ell_1^2 I_1 + \ell_2^2 I_2 + \ell_3^2 I_3.
\tag{12}
$$

Dimensional considerations dictate that the three constitutive parameters, ℓ_i, have dimensions of length.

The reader is referred to previous work [12,15] for full details of the version of strain gradient plasticity theory that was employed here for the calculations of both indentation and crack growth. The phenomenological constitutive model adopts isotropic hardening, which is tied to increments in the generalized effective plastic strain, and normality of plastic straining associated with an isotropic yield surface. The theory reduces to the classical J_2 flow theory of plasticity in the limit when the gradients are small; i.e. when terms such as $\ell_1^2 I_1$ in Equation (12) are small compared to $\dot{\varepsilon}_p^2$.

2.2. *The role of the length parameters in indentation*

Earlier work [15–19] has suggested that ℓ_1 is the dominantly important length parameter in two closely related problems: indentation and void growth. In spherically symmetric void growth, ℓ_2 has no influence. (Individual length parameters matter. For example,
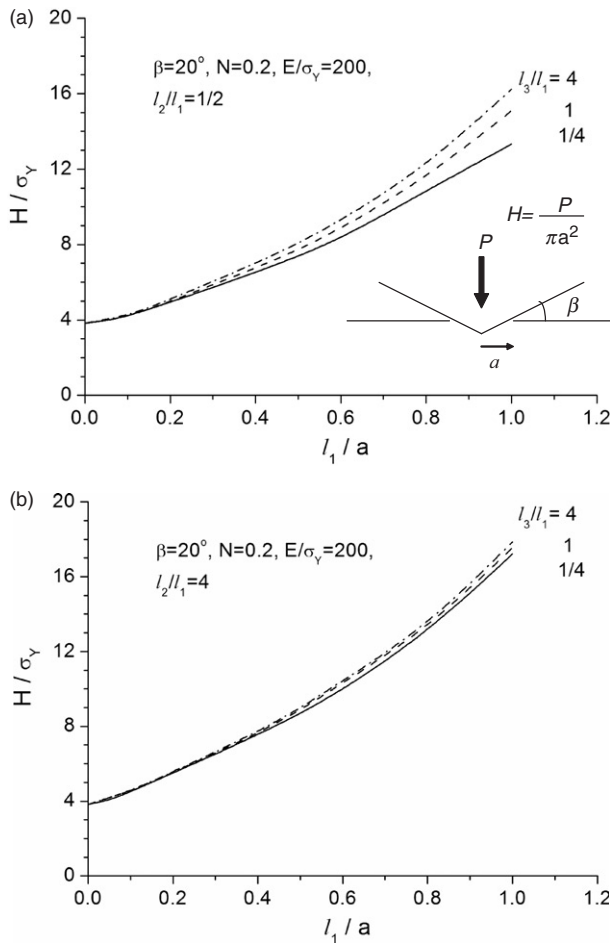
Figure 2. The role of the three material length parameters in hardness for conical indentation: (a) $\ell_2/\ell_1 = 1/2$; (b) $\ell_2/\ell_1 = 4$. The uniaxial stress–strain curve is specified by the power law of Equation (3) with $\sigma_Y/E = 1/200$ and $N = 0.2$.

wire torsion depends only on ℓ_2 [15].) Here, a new set of results is presented in Figure 2 computed with the present plasticity model that highlights the dominant importance of ℓ_1 for indentation. In Figure 2, ℓ_3 ranges from $\ell_1/4$ to $4\ell_1$, with $\ell_2 = \ell_1/2$ in Figure 2a, and $\ell_2 = 4\ell_1$ in Figure 2b. Whereas the effects of ℓ_2 and ℓ_3 are not negligible, even large changes of these length parameters give rise to relatively small changes in hardness compared to comparable changes generated by ℓ_1.

2.3. *The role of the three length parameters in crack growth*

The results in Figure 3 were computed using a modified version of the unified model to illustrate the roles of the three length parameters on the steady state toughness, Γ_{SS}. It will be argued that the situation is similar to that noted above for indentation: *the length*
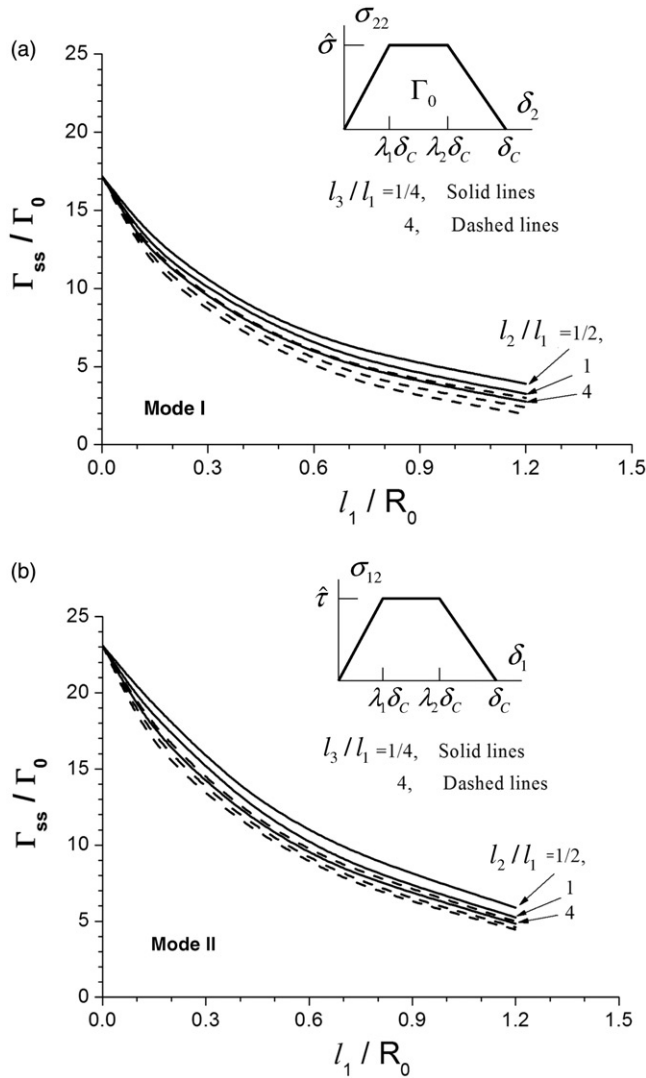
Figure 3. Dependence of interface toughness on material length parameters as predicted by the unified model. The traction–displacement relation linking identical blocks of material on either side of the interface is shown in the insert: in (a) for mode I, $\hat{\sigma}/\sigma_Y = 10$; in (b) for mode II, $\hat{\tau}/\sigma_Y = 10$. In all cases, $\sigma_Y/E = 1/200$, $\nu = 0.3$, $N = 0.2$, $D/R_0 = 0.04$, $\lambda_1 = 0.15$ and $\lambda_2 = 0.5$. The interface separation energy is $\Gamma_0 = (1 - \lambda_1 + \lambda_2)\hat{\sigma}\delta_C/2$ in (a) and $\Gamma_0 = (1 - \lambda_1 + \lambda_2)\hat{\tau}\delta_C/2$ in (b).

parameter of dominant importance is ℓ_1. The two sets of results in Figure 3 apply to crack grow between identical elastic-plastic solids above and below the interface, with parameters specified in the figure caption. The dislocation-free strip is inserted above and below the interface such that its total thickness is $2D$. Figure 3a gives results for mode I growth in which the fields are symmetric about the interface, whereas Figure 3b presents the results for pure mode II such that the fields are anti-symmetric. For these

calculations, we have used the specific traction–separation relation [6] shown in the insert in each figure. In mode I, the shear traction is zero, while in mode II the normal traction is zero; an uncoupled relation can be used in each case. The cohesive work/area required to fail the interface, Γ_0, is the area under the traction-separation curve. The mode II case models a "shearing failure" of the interface with no separation taking place.

The results for the cases shown in Figure 3 were computed with $D/R_0 = 0.04$. This particular set of material and interface parameters is representative and the results show that the macroscopic interface toughness, Γ_{SS}, can be many times the interface energy, Γ_0. This large toughness enhancement is due to plastic dissipation accompanying interface separation (or interface shear failure in mode II), as alluded to in the Introduction. The larger the material length parameter, as measured by ℓ_1/R_0, the smaller the enhancement due to the fact that strain gradient hardening makes it easier to attain the peak traction, $\hat{\sigma}$ (or $\hat{\tau}$), needed to fail the interface. The limit of Γ_{SS}/Γ_0 as $\ell_1/R_0 \to 0$, corresponding to convention plasticity, is strongly dependent on D/R_0. It is unbounded if $D/R_0 = 0$ because the stresses on the interface from conventional plasticity can never reach the peak separation stresses used in these examples. Indeed, this was the motivation in earlier work [5,7] for the introduction of the dislocation-free strip. The dependence of the interface toughness on D/R_0 when strain gradient plasticity is in force will be evaluated in the next section.

Of primary interest in this section is the dependence of Γ_{SS}/Γ_0 on the material length parameters. Figure 3 reveals that ℓ_2 and ℓ_3 have a much smaller influence on Γ_{SS}/Γ_0 than ℓ_1 for both mode I and mode II, although their effect is not negligible as noted for indentation. Results presented henceforth in this paper for both indentation and crack growth have been computed with the ratios of the length parameters fixed according to $\ell_2 = \ell_3 = \ell_1 \equiv \ell$, with ℓ regarded as the primary length parameter ℓ_1. Computations fitted to indentation data for the Ni-alloy will be used to determine the length parameter, ℓ.

3. Interface separation

In this section, recent results for normal and mixed mode atomistic separation of a specific Al_2O_3/Ni interface computed using density functional theory [2,3] will be used to motivate the introduction of an interface potential governing mixed mode traction–separation. The potential introduced in Section 1 can be fit to data from atomistic calculations for normal separation and either constrained or unconstrained shear.

For interface separations without plane strain conditions enforced, the following notation is used for the traction components on the interface, which is normal to the x_2 direction, and the displacement components of the block of material above the interface relative to those of the block below:

$$(T_1, T_2, T_3) \equiv (\sigma_{12}, \sigma_{22}, \sigma_{32}) \text{ and } (\delta_1, \delta_2, \delta_3). \tag{13}$$

These variables are conjugate to each other in the sense that the increment of work/area due to an increment of relative displacement is

$$dW = T_1 d\delta_1 + T_2 d\delta_2 + T_3 d\delta_3. \tag{14}$$

Traction–displacement results [2,3] for the Ni/Al_2O_3 interface are presented in Figure 4 for normal (mode I) separation (Figure 4a), for constrained shearing across the interface
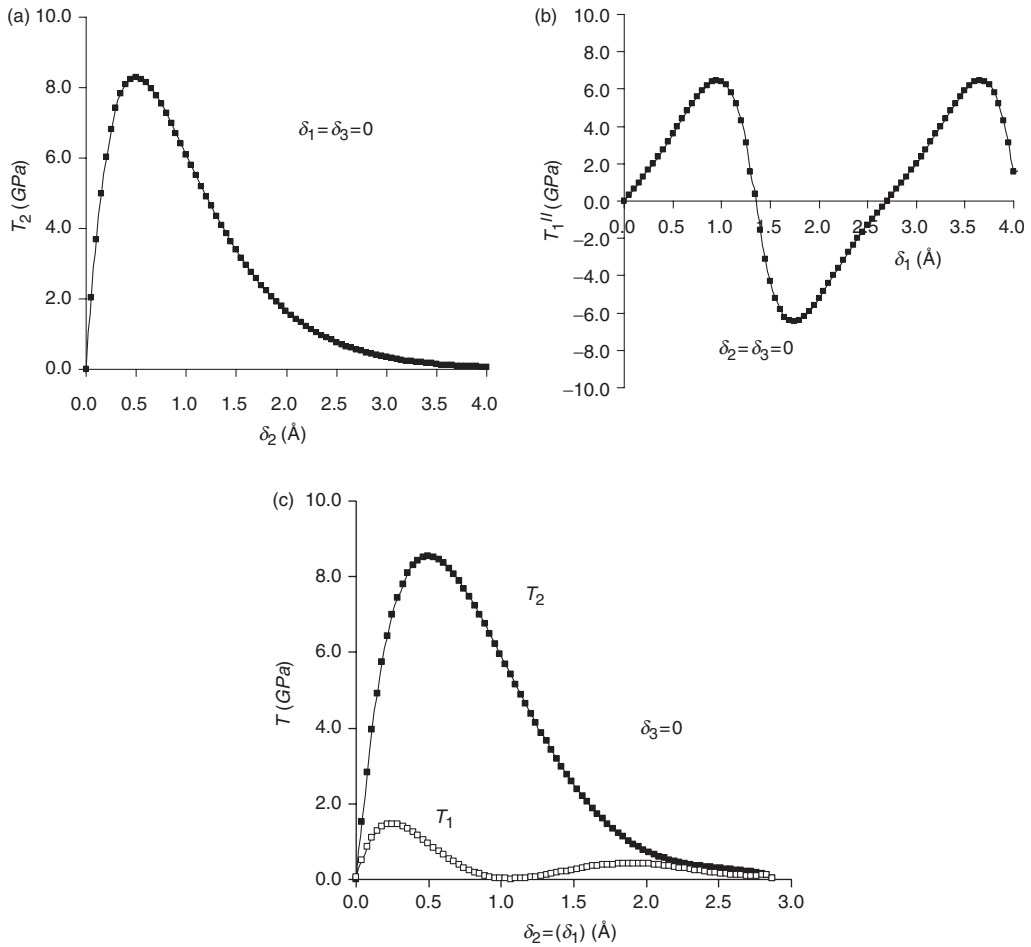
Figure 4. Atomistic traction–displacement results from Jiang and Smith [3] for the Al_2O_3/Ni interface: (a) normal separation; (b) constrained shear; (c) 45° separation.

(mode II) (Figure 4b) and for a mixed mode case with $\delta_2 = \delta_1$ (referred to as 45° separation) (Figure 4c). The particular interface taken in this study is the relatively weak stoichiometric interface joining the {111} plane of γ-Ni to the {0001} plane of α-Al_2O_3 terminated by Al atoms. The x_1-direction coincides with the $\langle 110 \rangle$ direction of the γ-Ni {111}. Positions of Ni atoms within two layers of the interface are relaxed in the calculations, whereas two layers of O atoms and four layers of Al atoms from the interface are relaxed. Outside these layers the atoms are displaced rigidly. The displacements in Equation (13) are the relative displacements of the rigid blocks. In all three cases in Figure 4, δ_3 is constrained to be zero. In normal separation, symmetry dictates that both δ_1 and δ_3 are zero. In the constrained shear computations, δ_2 is taken to be zero, whereas for 45° separation, $\delta_2 = \delta_1$. (The atomistic results for shear and mixed mode separation should be regarded as preliminary. Whereas the imposed constraints are compatible with the present model, further atomistic calculations [3] will be carried out to establish to what
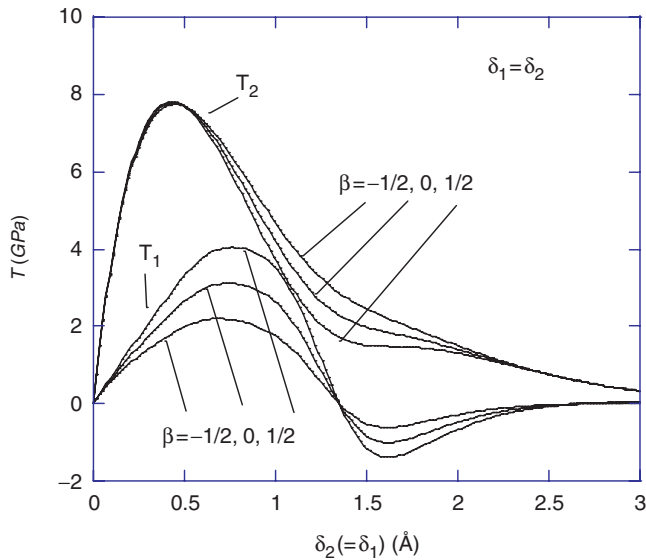
Figure 5. Traction–displacement results from the interface potential for three values of β, which can be compared with the corresponding results from the atomistic calculations of Jiang and Smith [3] in Figure 4c. With $\beta = 0$, the function $f(x)$ reproduces the constrained shear data from Figure 4b. In addition, $\Gamma_0 = 1.13\,\mathrm{J\,m^{-2}}$, $\hat{\delta} = 0.50\,\text{Å}$ and $b = 2.70\,\text{Å}$, reproducing the normal separation results in Figure 4a.

extent the results for shear and for 45° separation are sensitive to these constraints. Specifically, calculations for shear will be determined with no constraint normal to the interface. In principle, the potential, Equation (1), can be fit to either the constrained or unconstrained shear data).

In the atomistic modelling of the Ni/Al$_2$O$_3$ interface [2,3], atoms close to the interface relax their positions during separation but do not exchange positions nor are dislocations formed. Consequently, the work of separation, Γ_0, is path-independent; i.e. independent of the mode of separation. For the interface in Figure 4, $\Gamma_0 = 1.13\,\mathrm{J\,m^{-2}}$, and for normal separation in Figure 4a, $\hat{\delta} = 0.50\,\text{Å}$ ($\hat{\sigma} = 8.3\,\mathrm{GPa}$). With these choices, the traction–separation curve generated by the potential, Equation (1), is essentially indistinguishable from the computed curve. In constrained shearing with $\delta_2 = 0$, separation does not occur and $T_1^{II}(\delta_1)$ in Figure 4b has period $b = 2.70\,\text{Å}$. The function $f(\delta_1)$ ensuring that the potential reproduces $T_1^{II}(\delta_1)$ is determined using Equation (4). Data for $T_2(\delta_1)$ for constrained shearing has not yet been computed and thus it was not possible to identify β. The choice $\beta = 0$ was made arbitrarily; however, it will be shown that β has relatively little influence on the mode I macroscopic toughness of this interface.

Traction–displacement results for 45° separation (with $\delta_1 = \delta_2$) computed from the potential, Equation (1), are presented in Figure 5. These can be compared with the atomistic calculations in Figure 4c. The curves for $\beta = \pm 1/2$ were computed with $f(\delta_1)$ determined with $\beta = 0$, as described above. Of the three values of β shown in Figure 5, the choice $\beta = -1/2$ appears to give the best representation of the separation data. The potential reasonably approximates the atomistic results for this particular mixed mode separation. The most important feature is almost certainly the fact that the peak normal

traction under $45°$ separation is almost as large as under a normal separation, and this feature is accurately replicated by the potential.

4. Interface toughness

The parameters ($\Gamma_0 = 1.13\,\mathrm{J\,m^{-2}}$, $\hat{\sigma} = 8.3\,\mathrm{GPa}$, $\hat{\delta} = 0.50\,\text{Å}$) and shear function specifying the interface potential are detailed in Section 3. The properties of the Ni alloy and Al_2O_3 are taken to be

$$
\begin{aligned}
&E_1 = 170\,\mathrm{GPa}, \ \nu_1 = 0.3, \ \sigma_Y = 700\,\mathrm{MPa}, \ N = 0.2, \ \ell \cong 50\,\mathrm{nm} \\
&E_2 = 400\,\mathrm{GPa}, \ \nu_2 = 0.2 \,,
\end{aligned}
\tag{15}
$$

where σ_Y and N as defined by Equation (10) were chosen to fit tensile stress–strain data for the bond coat alloy [20]. The length parameter, ℓ, in the strain gradient plasticity is approximately 50 nm obtained by fitting computed indentation results in Section 2.2 to indentation data [21], but ℓ will be treated as a free parameter in some of the results to follow. The reference length, Equation (8), is $R_0 = 46.2\,\mathrm{nm}$ and the ratio of peak normal stress to yield stress is $\hat{\sigma}/\sigma_Y = 11.86$. The remote boundary on which the elastic field characterized by K_I and K_II is imposed is taken as $R_\mathrm{remote} = 1000\,R_0$ with implications discussed later.

4.1. The roles of β and D

The results in Figure 6 for mode I interface toughness will be used to establish those aspects of the toughness model that are the important and those that can be ignored. The normalized toughness, Γ_{SS}/Γ_0, plotted as a function of D/R_0 in Figure 6 has been computed using the unified model with $\ell/R_0 = 1$. The enhancement of interface toughness by plasticity is reflected in the amplification of Γ_{SS}/Γ_0 above unity. Results for both $\beta = 0$ and $\beta = -1/2$ are presented indicating that this interface parameter plays a minor role in determining mode I toughness; $\beta = -1/2$ will be used in the sequel. A second set of curves has been computed to show the effect of a lower interface strength, $\hat{\sigma} = 7.0\,\mathrm{GPa}$ ($\hat{\delta} = 0.593\,\text{Å}$), with the work of separation unchanged at $\Gamma_0 = 1.13\,\mathrm{J\,m^{-2}}$. Clearly, the interface strength is a major factor underlying toughness independent of the work of separation. It will also be evident that the material length, ℓ, is another major factor.

Of particular significance in Figure 6 is the finding that Γ_{SS}/Γ_0 becomes independent of the height, D, of the elastic strip imposed between the interface and the plastic zone if $D/R_0 < 0.02$. As previously remarked, dislocations are not emitted at the crack tip between Ni and Al_2O_3 eliminating the possibility of crack tip blunting due to dislocation emission. The fact that Γ_{SS}/Γ_0 becomes independent of D suggests that near-tip dislocations are relatively unimportant in determining the toughness of this interface. The reasons for this are two-fold. First, strain gradient plasticity by itself is sufficient to elevate the near-tip stresses to levels required to separate the interface. Secondly, the steady-state toughness is associated with extensive crack advance (compared to the active plastic zone size) in which the macroscopic energy release, $G = \Gamma_{SS}$, is the sum of the work of separation and plastic dissipation. Because the plastic zone height, $\approx (\Gamma_{SS}/\Gamma_0)R_0$, is orders of magnitude greater than D, the dissipation occurring within the region
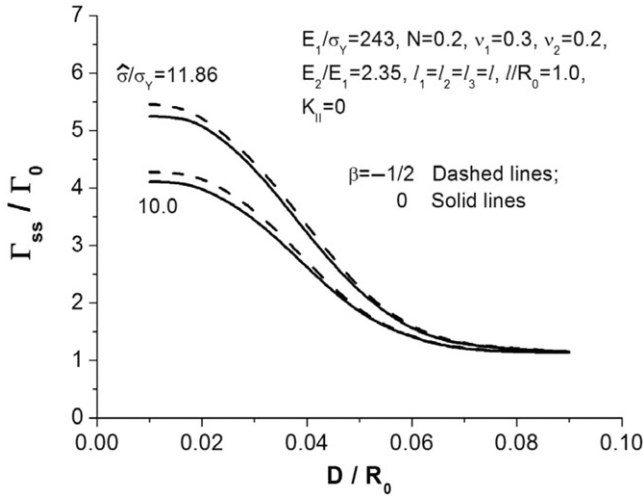
Figure 6. Mode I interface toughness normalized by interface separation energy as a function of the width of the elastic region between the interface and the plastic zone as predicted by the unified model. The curves have been computed with the properties of Ni and Al_2O_3 given in the text with $\Gamma_0 = 1.13 Jm^{-2}$ and the interface potential fit to the pure shear behavior in figure 4b. The curves with $\hat{\sigma}/\sigma_Y = 11.86$ ($\hat{\sigma} = 8.3 GPa$, $\hat{\delta} = 0.5 Å$) correspond to the Ni/Al_2O_3 interface. The parameter β characterizing the coupling with the normal stress in pure shear of the interface has little influence on the interface toughness. The curves for $\hat{\sigma}/\sigma_Y = 10$ ($\hat{\sigma} = 7.0 GPa$, $\hat{\delta} = 0.59 Å$) reflect the effect of a reduction in interface strength with unchanged work of separation, Γ_0. The toughness predictions become independent of D if $D/R_0 < 0.02$.

$D < 0.02R_0$ can be neglected. By contrast, plasticity enhancement of the toughness is largely suppressed, with $\Gamma_{SS}/\Gamma_0 \to 1$, if $D/R_0 > 0.06$ because then the bending stiffness of elastic strip becomes sufficient to shut down most of the shearing deformation within the plastic zone.

4.2. *The length of the separation zone*

The length of the zone over which separation of the interface takes place, L_{coh}, is not known in advance and must be computed. It is defined as the distance between the crack tip, where the tractions effectively vanish (taken as $\delta_2 > 8\hat{\delta}$), and the point ahead of the peak normal traction where $\delta_2 = \hat{\delta}/4$. Figure 7 plots the normalized length, $L_{\text{coh}}/\hat{\delta}$, as a function of ℓ/R_0 for two values of D/R_0. With $\ell/R_0 = 1$, corresponding to the results in the previous figure, L_{coh} is from 8 to 12 times $\hat{\delta}$, depending on D/R_0.

4.3. *The role of material length scale ℓ in determining interface toughness*

In the remaining computations, the model with $D = 0$ will be used, as proposed originally in [12]. The dependence of Γ_{SS}/Γ_0 on ℓ/R_0 and $\hat{\sigma}/\sigma_Y$ is presented in Figure 8 for mode I. Results for $\hat{\sigma}/\sigma_Y = 11.86$ ($\hat{\sigma} = 8.3 GPa$, $\hat{\delta} = 0.5 Å$) for the stoichiometric Ni/Al_2O_3
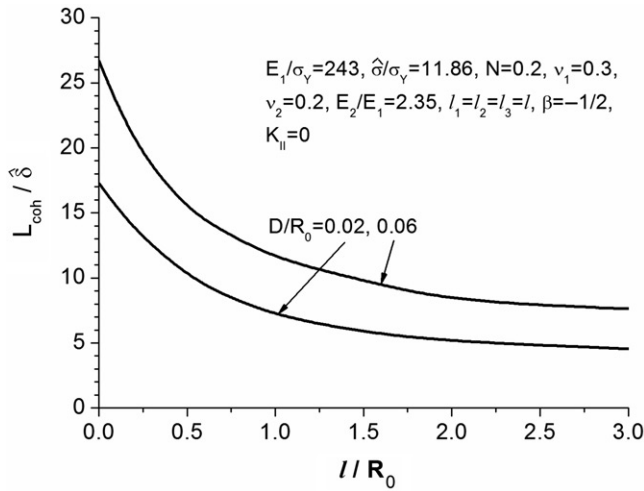
Figure 7. The length of the cohesive zone over which separation occurs in mode I.
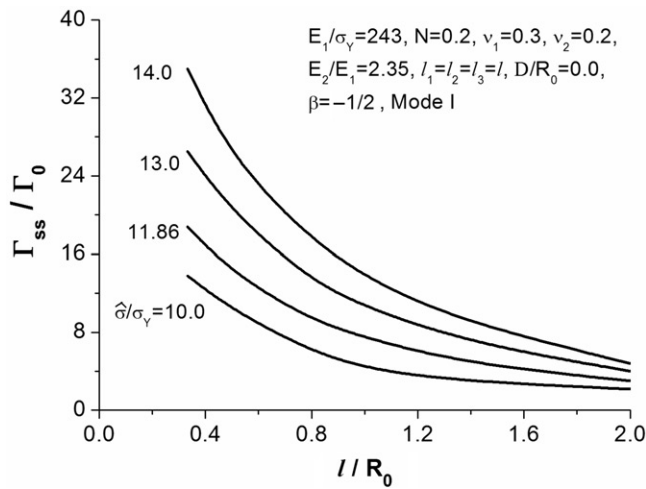

Figure 8. The effect of the plasticity length scale, ℓ, on the interface toughness in mode I computed with $D = 0$. The curves have been computed with the properties of Ni and Al$_2$O$_3$ given in the text with $\Gamma_0 = 1.13\,\mathrm{J\,m^{-2}}$ using the interface potential fit to the pure shear behavior in Figure 4b with $\beta = -1/2$. The curve with $\hat{\sigma}/\sigma_Y = 11.86$ ($\hat{\sigma} = 8.3\,\mathrm{GPa}$, $\hat{\delta} = 0.5\,\text{Å}$) correspond to the Ni/Al$_2$O$_3$ interface. The curves for other values of $\hat{\sigma}/\sigma_Y$ reflect the effect of a change in interface strength with unchanged work of separation, Γ_0.

interface are shown along with those for other interface strengths, in all cases with $\Gamma_0 = 1.13\,\mathrm{J\,m^{-2}}$. The strong effects of the material length scale and the interface strength on the interface toughness are evident. Larger values of ℓ/R_0 promote higher stress near the crack tip, reducing G required to separate the interface. As already remarked, the limit
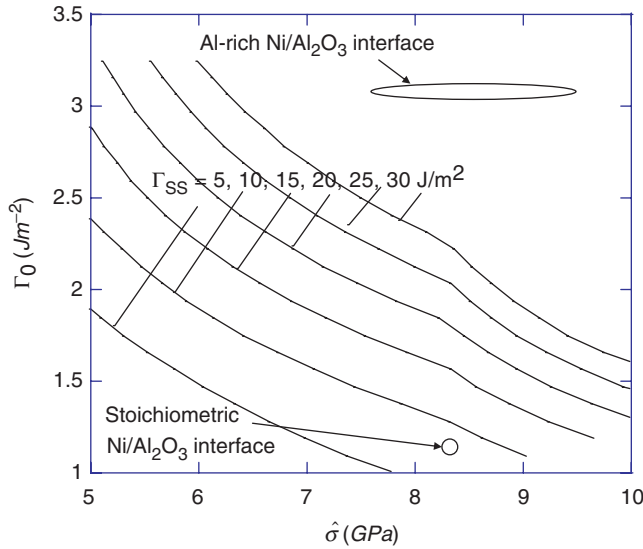
Figure 9. Dependence of the mode I interface toughness, Γ_{SS}, on the primary interface parameters, Γ_0 and $\hat{\sigma}$, for Ni alloy/Al$_2$O$_3$ systems. The elastic properties are specified in the text. The plasticity of the Ni is specified by $\sigma_Y = 700$ MPa, $N = 0.2$ and $\ell = 50$ nm.

$\ell/R_0 \to 0$ is conventional plasticity which is incapable of elevating stresses to the level required to separate the interface.

4.4. *The influence of* Γ_0 *and* $\hat{\sigma}$ *on mode I interface toughness*

Although the dimensionless results in Figure 8 were computed with $\Gamma_0 = 1.13$ J m^{-2}, they are valid for arbitrary values of Γ_0, as can be seen from the dimensionless form for Γ_{SS}/Γ_0 in Equation (9). Thus, by accounting for the dependence of both Γ_{SS}/Γ_0 and ℓ/R_0 on Γ_0 in Figure 8, these results can be used to construct the results in Figure 9 showing the dependence of Γ_{SS} on Γ_0 and $\hat{\sigma}$ over ranges of these interface properties relevant to most Ni alloy/Al$_2$O$_3$ systems. Figure 9 has been constructed with $\ell = 50$ nm. The point corresponding to the stoichiometric Ni/Al$_2$O$_3$ interface, is indicated in Figure 9, as is the likely range for an Al-rich Ni/Al$_2$O$_3$ interface, for which $\Gamma_0 \approx 3.1$ J m^{-2} [2,3] ($\hat{\sigma}$ is not yet available for the latter interface). Clearly, the stoichiometric interface is too weak to account for the macroscopic mode I toughness, $\Gamma_{SS} \approx 30$ J m^{-2}, measured for Ni alloy/Al$_2$O$_3$ interface of NiCoCrAlY thermal barrier coating systems prior to any significant deterioration of the interface [22,23]. On the other hand, the Al-rich Ni/Al$_2$O$_3$ interface exceeds the performance of the actual interface. The stoichiometric and the Al-rich interfaces appear to bracket the properties likely to pertain to the Ni alloy/Al$_2$O$_3$ interface of the thermal barrier coating system [2]. Segregates to these two limiting interfaces of various kinds have been considered by Smith et al. [2] giving rise to intermediate levels of the work of separation consistent with $\Gamma_{SS} \approx 30$ J m^{-2}. Details of the actual interface for the thermal barrier coating have not yet been established and they almost certainly change with thermal exposure. It is possible that the actual interface may
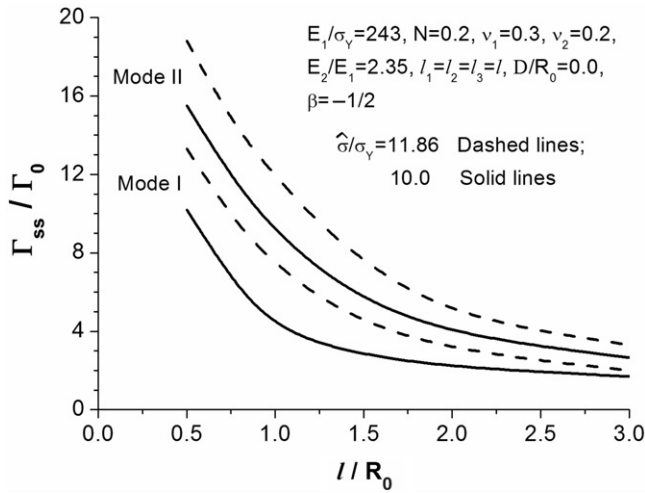
Figure 10. The effect of the plasticity length scale, ℓ, on the interface toughness in mode I and mode II. The curves have been computed with the properties of Ni and Al_2O_3 given in the text with $\Gamma_0 = 1.13 \, J \, m^{-2}$ and the interface potential fit to the pure shear behavior in Figure 4b. The curves with $\hat{\sigma}/\sigma_Y = 11.86$ ($\hat{\sigma} = 8.3 \, GPa$, $\hat{\delta} = 0.5 \, \text{Å}$) correspond to the stoichiometric Ni/Al_2O_3 interface. The curves for $\hat{\sigma}/\sigma_Y = 10$ ($\hat{\sigma} = 7.0 \, GPa$, $\hat{\delta} = 0.59 \, \text{Å}$) reflect the effect of a reduction in interface strength with unchanged work of separation, Γ_0.

be a mixture of patches of stoichiometric and Al-rich components. The importance of changes in Γ_0 and $\hat{\sigma}$, either deleterious or enhancing, are highlighted by Figure 9.

5. Mixed mode toughness

The role of the mode mix, $\psi = \tan^{-1}(K_{II}/K_I)$, on the interface toughness is displayed in Figures 10 and 11. Figure 10 compares mode II ($K_{II} > 0$, $K_I = 0$) with mode I as a function of ℓ/R_0. Figure 11 displays the dependence $\Gamma_{SS}(\psi)$ over the full range of ψ for the Ni/Al_2O_3 system with the stoichiometric interface and $\ell/R_0 = 1$. The general trend seen in these figures, whereby mixed mode loadings results greater interface toughness enhancement by plasticity, is similar to that seen in more generic models [24] and in experiments [25,26]. The dependence on mode in Figure 11 is not as large as in systems where plasticity enhancement of toughness is larger. We expect that a stronger dependence on mode would be seen for the Ni/Al_2O_3 system if $\hat{\sigma}/\sigma_Y$ were larger.

Recall that the elastic field, specified by (K_I, K_{II}), is imposed on a remote boundary a distance $R_{remote} = 1000 \, R_0$ from the crack tip. One of the consequences of the elastic mismatch between Ni and Al_2O_3 is the fact that the ratio of shear stress to normal stress acting on the interface depends on the distance from the crack tip. The second Dundurs' mismatch parameter, β_D, determines this dependence. In plane strain,

$$\beta_D = \frac{1}{2} \frac{\mu_1(1 - 2\nu_2) - \mu_2(1 - 2\nu_1)}{\mu_1(1 - \nu_2) + \mu_2(1 - \nu_1)}, \tag{16}$$
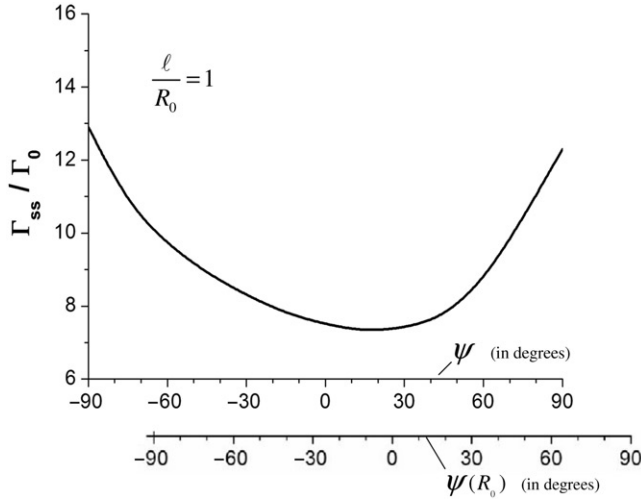
Figure 11. The effect of mode mix $\psi = \tan^{-1}(K_{II}/K_I)$ on the interface toughness. The curves have been computed with the properties of Ni and Al_2O_3 given in the text, with $\Gamma_0 = 1.13\,\mathrm{J\,m^{-2}}$ and $\hat{\sigma}/\sigma_Y = 11.86$ ($\hat{\sigma} = 8.3\,\mathrm{GPa}$, $\hat{\delta} = 0.5\,\mathrm{Å}$) corresponding to the stoichiometric Ni/Al_2O_3 interface with $\beta = -1/2$. The relation between the remote mode mix, ψ, and the mode mix a distance R_0 ahead of the crack tip (from elasticity), $\psi(R_0)$, is discussed in the text.

where $\mu = E/[2(1 + \nu)]$ is the elastic shear modulus. For the Ni/Al_2O_3 system,

$$\beta_D = -0.206 \text{ and } \varepsilon \equiv \frac{1}{2\pi}\ln\left(\frac{1 - \beta_D}{1 + \beta_D}\right) = 0.067. \tag{17}$$

In the present model, $\psi = \tan^{-1}(K_{II}/K_I)$, is equivalent to $\psi = \tan^{-1}(\sigma_{12}/\sigma_{22})$ as the measure of the ratio of shear stress to normal stress on the interface in the remote field a distance R_{remote} ahead of the tip. Define a similar measure of this ratio at any distance R ahead of the tip: $\psi(R) = \tan^{-1}(\sigma_{12}/\sigma_{22})$. From elasticity theory [27,28],

$$\psi(R) = \psi + \varepsilon \ln(R/R_{\mathrm{remote}}). \tag{18}$$

For the Ni/Al_2O_3 system with $R_{\mathrm{remote}} = 1000\,R_0$ and $R = R_0$, Equation (18) implies a shift in mode mix from remote to near-tip locations given by $\psi(R_0) = \psi - 26.5°$. Dependence of Γ_{SS} on the near-tip measure, $\psi(R_0)$, is included in Figure 11. Whereas other choices could have been made for the near-tip measure, the minimum in interface toughness is roughly coincident with the attainment of purely normal stressing of the interface in the vicinity of the tip. The shift to the local measure helps explain the asymmetry in the dependence of Γ_{SS} on mode mix. Other aspects of this asymmetry are due to the fact that different materials are joined at the interface and that only one of them deforms plastically.

6. Concluding remarks

Even though Ni/Al_2O_3 interfaces are relatively brittle with a plastic zone a micron or less in size, plasticity enormously enhances the macroscopic interface toughness. Indeed, plasticity accompanying interface fracture is essential to the adherence of thermal barrier

coatings. The model of interface toughness developed and analyzed in the paper establishes the highly nonlinear coupling between plastic dissipation and the atomistic work of separation, Γ_0, and normal strength of the interface, $\hat{\sigma}$, revealing that both are important. Relatively small changes in either interface property can result in significant changes in toughness at the macroscopic scale.

Whereas the primary emphasis in this paper has been on how the interface properties, Γ_0 and $\hat{\sigma}$, influence toughness, the results for the interface toughness model also reveal the important role of the Ni alloy plasticity properties. A decrease in yield strength, σ_Y, parlays into increased toughness in Figure 8 in two ways: (i) through a decrease in ℓ/R_0 because R_0 depends on $1/\sigma_Y^2$ and (ii) through an increase in $\hat{\sigma}/\sigma_Y$. Large gains in interface toughness can be achieved by reducing the yield strength of the Ni alloy, assuming this could be done without sacrificing interface properties. A reduction in the material length parameter, ℓ, also increases toughness although not as dramatically as a decrease in yield strength. Of all the Ni alloy material properties, the material length parameter, ℓ, is the most uncertain. Absolute levels of toughness computed here should be judged accordingly. However, the trends, such as those in Figures 8 and 9, showing relative changes in interface toughness with changes in the interface properties or the plasticity properties of the Ni alloy are less subject to uncertainty in ℓ.

A consequence of asymmetry induced by elastic mismatch between the two materials and plasticity on one side of the interface is that even a mode I loading induces some shearing behavior on the interface in the vicinity of the crack tip. Thus, a toughness model such as that introduced here must incorporate a mixed mode traction-separation law for the interface. Nevertheless, a mode I loading results in separation conditions on the interface that are nearly normal separation. For this reason, the results for mode I toughness, which comprise most of those presented in this paper, are not likely to be sensitive to the uncertainties surrounding the atomistic shearing and mixed mode separation computations mentioned in Section 3. It remains to be seen whether the trends in Figures 10 and 11 for mixed mode toughness will change significantly if the atomistic results for interface shear and mixed mode separation turn out to differ appreciably from the preliminary ones used here.

References

[1] T. Xu, S. Faulhaber, C. Mercer et al., Acta Mater. 52 (2004) p.1439.
[2] J.R. Smith, Y. Jiang and A.G. Evans, Int. J. Mater. Res. 98 (2007) p.1214.
[3] Y. Jiang and J.R. Smith, private communication (2008).
[4] Y. Wei and J.W. Hutchinson, Int. J. Fract. 95 (1999) p.1.
[5] Z. Suo, C.F. Shih and A.G. Varias, Acta Metall. Mater. 41 (1993) p.1551.

[6] V. Tvergaard and J.W. Hutchinson, J. Mech. Phys. Solids 40 (1992) p.1377.
[7] G.E. Beltz, J.R. Rice, C.F. Shih et al., Acta Mater. 44 (1996) p.3943.
[8] D.M. Lipkin, D.R. Clarke and G.E. Beltz, Acta Mater. 44 (1996) p.4051.
[9] Y. Sun, G.E. Beltz and J.R. Rice, Mater. Sci. Eng. A 170 (1993) p.67.
[10] A. Needleman, J. Mech. Phys. Solids 38 (1990) p.289.
[11] J.H. Rose, J. Ferrante and J.R. Smith, Phys. Rev. Lett. 47 (1981) p.675.
[12] Y. Wei and J.W. Hutchinson, J. Mech. Phys. Solids 45 (1997) p.1253.
[13] Y.G. Wei, Eur. J. Mech. A 25 (2006) p.897.
[14] N.A. Fleck, G.M. Muller, M.F. Ashby et al., Acta Metall. Mater. 42 (1994) p.475.
[15] N.A. Fleck and J.W. Hutchinson, Adv. Appl. Mech. 33 (1997) p.295.
[16] N.A. Fleck and J.W. Hutchinson, J. Mech. Phys. Solids 49 (2001) p.1847.
[17] M.R. Begley and J.W. Hutchinson, J. Mech. Phys. Solids 46 (1998) p.2049.
[18] Y. Wei and J.W. Hutchinson, J. Mech. Phys. Solids 51 (2003) p.2037.
[19] U. Komaragiri, S.R. Agnew, R.P. Gangloff, et al., to be published (2008).
[20] K.J. Hemker, B.G. Mendis and C. Eberl, Mater. Sci. Eng. A 483–484 (2008) p.727.
[21] K.J. Hemker, private communication (2007).
[22] F.G. Gaudette, S. Suresh and A.G. Evans, Metall. Mater. Trans. 31A (2000) p.1977.
[23] A.G. Evans, *Adhesion Measurement of Films and Coatings*, Vol. 2 (VSP BV, 2001), p.10.
[24] V. Tvergaard and J.W. Hutchinson, J. Mech. Phys. Solids 41 (1993) p.1119.
[25] K.M. Liechti and Y.S. Chai, J. Appl. Mech. 59 (1992) p.295.
[26] L. Banks-Sills, V. Boneiface and R. Eliasi, Int. J. Solids Struct. 42 (2005) p.663.
[27] J.R. Rice, J. Appl. Mech. 55 (1988) p.98.
[28] J.W. Hutchinson and Z. Suo, Adv. Appl. Mech. 29 (1992) p.63.